

Tuning the Electronic and Optical Properties of Graphene via Doping to Realize Nitrogen Dioxide Sensing: A Computational Study

Lei Luo, Hongqiang Zhu,* Kaihui Yin, Zebang Wu, Fengxia Xu, Tianjun Gao, Yuanxia Yue, Jianjun Chen, Qing Feng, Ying Yang, and Weiyao Jia*



Cite This: *ACS Omega* 2025, 10, 1486–1492



Read Online

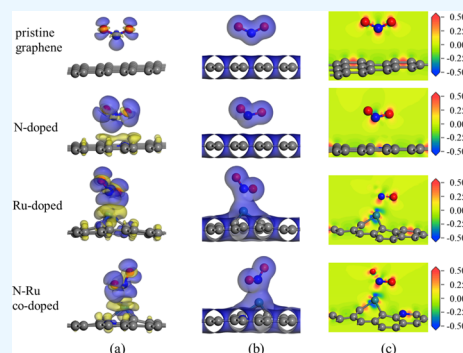
ACCESS |

Metrics & More

Article Recommendations

Supporting Information

ABSTRACT: Recently, doped graphene has emerged as a promising material for gas sensing applications. In this study, we performed first-principles calculations to investigate the adsorption of nitrogen dioxide (NO_2) on pristine, nitrogen (N)-doped, ruthenium (Ru)-doped, and N–Ru-co-doped graphene surfaces. The adsorption energies, Mulliken charge distributions, differential charge densities, electronic density of states, and optical properties of NO_2 on the graphene surfaces were evaluated. The adsorption energies follow the order N–Ru-co-doped > Ru-doped > N-doped > pristine graphene, suggesting that doped graphene has higher sensitivity to NO_2 gas molecules than pristine graphene. Analysis of the charge transfer and differential charge densities indicated weak physisorption of NO_2 on pristine and N-doped graphene, whereas stronger chemisorption of NO_2 occurred on Ru-doped and N–Ru-co-doped graphene because of the formation of chemical bonds between NO_2 and the doped surfaces. The peak absorption and reflection coefficients of NO_2 adsorbed on N–Ru-co-doped graphene are approximately 2.88 and 7.75 times higher, respectively, than those of NO_2 adsorbed on pristine graphene. The substantial changes of the electronic and optical properties of N–Ru-co-doped graphene upon interaction with NO_2 can be exploited for the development of highly sensitive and selective NO_2 gas sensors.



1. INTRODUCTION

Environmental pollution has reached alarming levels because of the rapid advance of modern industrialized society. A pollutant of considerable concern is nitrogen dioxide (NO_2), which is a toxic and hazardous gas that poses a substantial threat to human health and the environment.¹ As a major atmospheric contaminant, NO_2 infiltrates the ozone layer, catalyzes atmospheric degradation, and reacts with oxygen and water vapor to form nitric acid, which corrodes plants and materials such as metals and concrete, leading to soil acidification and decreased fertility.^{2–5} Moreover, NO_2 can damage the human liver, kidneys, and respiratory system, and it can be fatal in severe cases.^{6–8} Consequently, the detection and capture of NO_2 gas molecules are of great importance for environmental monitoring, industrial chemical processing, public safety, agriculture, medicine, and indoor air quality control.

Over the past few years, ultrathin two-dimensional (2D) materials have attracted remarkable interest owing to their unique structural, optoelectronic, mechanical, and thermal properties.^{9–11} The excellent sensing properties of some 2D materials, such as graphene and MoS_2 , have been demonstrated by theoretical and experimental studies.^{12–14} One of the most popular 2D layered materials is graphene, which consists of sp^2 -hybridized carbon atoms in a honeycomb lattice. Graphene has excellent optical, electrical, and thermal

properties, high carrier mobility, large specific surface area, low electrical noise, and the ability to detect various gas molecules with high resolution even at room temperature, and it has thus been widely investigated as a promising material for gas sensing.^{15–18} However, the pristine graphene surface is chemically inert, and the zero band gap of graphene decreases its sensitivity to gas molecules.^{19,20} To overcome these limitations and substantially improve its sensing performance, graphene can be modified by adding impurity atoms to its surface, such as B, N, S, and Si dopants, which strengthens the interaction between graphene and common gases (e.g., CO , CO_2 , COCl_2 , and O_2).^{21–27} Doping graphene with transition metals (e.g., Fe, Co, Ni, Ru, Mo, Ti, Ga, Mn, and Pt) also improves its ability to adsorb gases such as O_2 , SO_2 , COCl_2 , and NH_3 .^{28–31} Accordingly, adsorption and sensing applications of doped graphene have become research hotspots. However, there have only been a few studies on the gas-sensing capability of nonmetal and metal codoped graphene. In this study, we investigated the adsorption of NO_2 molecules on the

Received: October 8, 2024
Revised: December 12, 2024
Accepted: December 18, 2024
Published: December 30, 2024



surfaces of pristine, nonmetal (N)-doped, metal (Ru)-doped, and nonmetal (N)–metal (Ru) codoped graphene by dispersion-corrected density functional theory (DFT) simulations and calculated the geometric, energetic, electronic, and optical properties of the systems. By extending the investigation of doped graphene in the field of adsorption and sensing applications, this study will provide theoretical support for research on graphene-based sensor materials.

2. MODEL CONSTRUCTION AND CALCULATION METHOD

All of the DFT calculations to investigate the interaction between NO₂ gas molecules and the graphene surfaces were performed with the CASTEP code. To ensure the accuracy of the calculations, the calculations incorporated the Grimme dispersion correction with the Perdew–Burke–Ernzerhof exchange–correlation functional under the generalized gradient approximation, accounting for the effects of the dispersion interactions, long-range electronic correlation effects, and van der Waals forces.^{32,33} The geometry optimizations were performed using the plane-wave ultrasoft pseudopotential method, where the ionic potentials are replaced with pseudopotentials that describe the electron–ion interactions. The Kohn–Sham equations and energy functionals were solved through self-consistency. A 4 × 4 × 1 supercell model of each graphene surface consisting of 32 atoms was constructed to prevent interlayer interactions. A vacuum layer of 20 Å was introduced, and the plane-wave truncation energy was set to 430 eV. The atomic force convergence accuracy was set to 0.03 eV/Å to ensure accurate calculations. The energy self-consistency accuracy converged to 5 × 10^{−7} eV/atom and the intra-atomic stress was maintained at 0.05 GPa. The Brillouin zone *k*-point grid was set to 4 × 4 × 1 to adequately sample the system.

To investigate whether the doped graphene structure is stable, we calculated the binding energy (E_b)

$$E_b = E_{(G+C)} - E_{(C)} - E_{(G)} \quad (1)$$

where $E_{(G+C)}$ is the energy of the doped system, $E_{(C)}$ is the energy of a single dopant atom, and $E_{(G)}$ is the energy of the vacant graphene corresponding to the number of dopant atoms.³⁴ When E_b is negative, the doped structure is stable.

To study the adsorption state of NO₂ on the doped graphene sheets, the adsorption energy of NO₂ (E_{ads}) was calculated by

$$E_{ads} = E_{gas+graphene} - (E_{graphene} + E_{gas}) \quad (2)$$

where E_{gas} is the energy of a single NO₂ gas molecule, $E_{graphene}$ is the energy of graphene without adsorbed NO₂ molecules, and $E_{gas+graphene}$ is the total energy of the whole adsorption system.³⁵ When E_{ads} is positive, the energy of the system is high and adsorption is energetically unfavorable. When E_{ads} is negative, the adsorption process is exothermic, the energy of the system decreases, the structure is stable, and adsorption readily occurs.

3. RESULTS AND DISCUSSION

Three adsorption sites were considered for the adsorption of NO₂ on the graphene surfaces: the top site above a carbon atom (T), the center of a carbon ring (H), and the bridge site above a C–C bond (B). Through calculation, the orientation of the NO₂ molecule was chosen to have the N atom facing

downward with an initial adsorption distance of 3 Å, as shown in Figure 1. Based on the combinations of the adsorption sites and doped atoms, a total of 14 models were constructed.

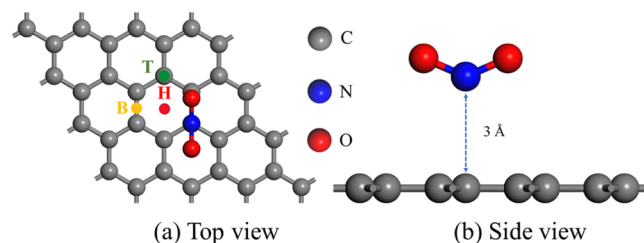


Figure 1. (a) Top view and (b) side view of a NO₂ molecule adsorbed on the surface of pristine graphene.

3.1. Adsorption Distance and Adsorption Energy.

According to the adsorption distances and E_{ads} values (Table S1), the H site was found to be the most stable site for NO₂ adsorption among the three sites. Therefore, here, we focus on the data for the H site. The data for the other two sites are provided in the Supporting Information. The atomic structures of NO₂ molecules adsorbed on the pristine and doped graphene surfaces after optimization are shown in Figure 2.

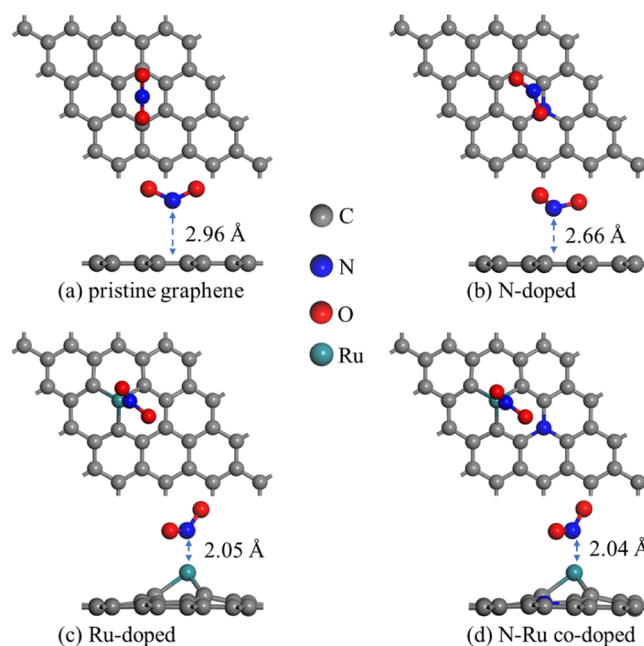


Figure 2. Top and side views of NO₂ adsorbed on (a) pristine graphene, (b) N-doped graphene, (c) Ru-doped graphene, and (d) N–Ru-co-doped graphene.

The adsorption distances before and after the adsorption of NO₂ molecules, E_{ads} values, and E_b values of the doped graphene surfaces are given in Table 1. The E_b values for the doped graphene surfaces are all negative, indicating that the doped graphene structures are stable. This provides a solid foundation for the subsequent adsorption of NO₂ molecules on the doped graphene surfaces.

The adsorption energies (E_{ads}) of all of the models are negative, indicating that the systems become more stable and have lower energy after NO₂ adsorption. According to the literature, $E_{ads} > 0.8$ eV indicates chemisorption, whereas $E_{ads} <$

Table 1. Pre-adsorption Distances (d_{pre}), Post-adsorption Distances (d_{post}), Adsorption Energies (E_{ads}), and Binding Energies (E_{b}) of NO₂ on the Different Graphene Surfaces

model	$d_{\text{pre}}/\text{\AA}$	$d_{\text{post}}/\text{\AA}$	E_{ads}/eV	E_{b}/eV
pristine graphene	3	2.96	-0.22	
N-doped	3	2.66	-0.69	-15.43
Ru-doped	3	2.05	-7.20	-6.29
N-Ru codoped	3	2.04	-7.41	-19.73

0.6 eV indicates physisorption.³⁶ Based on these criteria, it can be inferred that NO₂ molecules physisorb on pristine and N-doped graphene, suggesting weak adsorption of NO₂ on these graphene surfaces. In contrast, E_{ads} of NO₂ on Ru-doped and N-Ru codoped graphene exhibited a significant change from that on pristine graphene (approximately -0.2 eV) to approximately -7 eV. The magnitude of E_{ads} suggests strong interactions between the Ru-doped and N-Ru codoped graphene surfaces and NO₂ gas molecules, indicating chemisorption. Furthermore, the distances between the NO₂ molecules and these two graphene surfaces are smaller than that between pristine graphene and NO₂. Considering E_{ads} and the adsorption distances, it can be inferred that chemical bonds form between the Ru-doped and N-Ru codoped graphene surfaces and NO₂ molecules.

3.2. Charge Transfer Analysis. The Mulliken charge distributions of the NO₂ molecules adsorbed on the different graphene surfaces are given in Table 2. All of the surfaces undergo charge transfer with the NO₂ molecules. The amount of charge transfer follows the order N-Ru-co-doped graphene > Ru-doped graphene > N-doped graphene > pristine graphene. These results indicate that NO₂ acts as an electron acceptor in the charge transfer process, indicating reduction of NO₂ by the graphene surface. Additionally, the bond lengths of the NO₂ molecules are affected by adsorption on the graphene surfaces. The observed charge transfer and changes of the NO₂ molecule bond lengths indicate strong interactions between the doped graphene surfaces and NO₂ molecules. Strong interactions are beneficial for gas sensing because they lead to high sensitivity of the doped graphene surface for NO₂.

The charge density difference (CDD), total charge density (TCD), and electron density difference (EDD) plots of the NO₂ molecules adsorbed on the pristine and doped graphene surfaces are shown in Figure 3. The CDD plots clearly show

substantial charge transfer between the pristine and doped graphene surfaces and adsorbed NO₂ molecules. During the adsorption process, charge accumulation occurs on the NO₂ gas molecules and charge dissipation occurs at the adsorption sites on the graphene surfaces. Analysis of the TCD maps shown in Figure 3b and EDD plots shown in Figure 3c revealed that the electron orbitals of the pristine and N-doped graphene surfaces do not markedly overlap with those of NO₂, indicating weak interactions between these surfaces and the NO₂ molecules. In contrast, the electron orbitals of the Ru-doped and N-Ru-co-doped graphene surfaces clearly overlap with those of NO₂, suggesting the formation of chemical bonds between these surfaces and the gas molecules. These observations confirm the strong interactions between NO₂ and the Ru-doped and N-Ru-co-doped graphene surfaces. These findings align with E_{ads} and the Mulliken charge predictions for the interaction of NO₂ molecules with the different graphene surfaces.

3.3. Surface Electron State Density. To further analyze the electronic energies of the graphene-based systems after the adsorption of NO₂ molecules, the density of states (DOS) was calculated following the adsorption of a NO₂ molecule on each of the different surfaces (Figure 4). The DOSs of the doped surfaces generally shift toward the valence band compared with that of the pristine graphene surface. Additionally, the number of wave peaks in the valence band increases and the number of wave peaks in the conduction band decreases after doping of the graphene surface. The peaks from the impurity energy levels near the Fermi level also change after doping of the graphene surface. These phenomena suggest that the electronic properties of the doped systems are different from those of pristine graphene. This can be attributed to the electronic hybridization of the dopant atoms, as shown in Figure 4d, where the synergistic interaction of the 2p and 4d electrons of N and Ru with the 2p electrons of C atoms modifies the DOS of the codoped system. These changes of the DOS, particularly in the region near the Fermi level, affect the electronic properties of the doped systems, which is advantageous for sensing applications.

3.4. Optical Properties. The dielectric functions, absorption spectra, and reflection spectra of the four graphene-based systems were calculated before and after NO₂ adsorption. The optical properties of a material can be

Table 2. Mulliken Charge Distributions of the NO₂ Molecules before and after Adsorption on the Different Graphene Surfaces

model	species	selection	p electron	total	charge/e	molecular charge/e	population	bond length/\AA
NO ₂	N	1.39	3.18	4.57	0.44	0	0.68	1.23
	O	1.85	4.36	6.22	-0.22			
	O	1.85	4.36	6.22	-0.22			
pristine graphene	N	1.46	3.21	4.67	0.33	-0.25	0.63	1.24
	O	1.86	4.44	6.29	-0.29			
	O	1.86	4.44	6.29	-0.29			
N-doped	N	1.51	3.23	4.74	0.26	-0.48	0.60	1.25
	O	1.86	4.53	6.39	-0.38			
	O	1.86	4.51	6.36	-0.36			
Ru-doped	N	1.47	3.37	4.84	0.16	-0.49	0.67	1.27
	O	1.87	4.47	6.34	-0.34			
	O	1.86	4.45	6.31	-0.31			
N-Ru codoped	N	1.47	3.37	4.84	0.16	-0.51	0.67	1.27
	O	1.87	4.49	6.36	-0.36			
	O	1.86	4.45	6.31	-0.31			

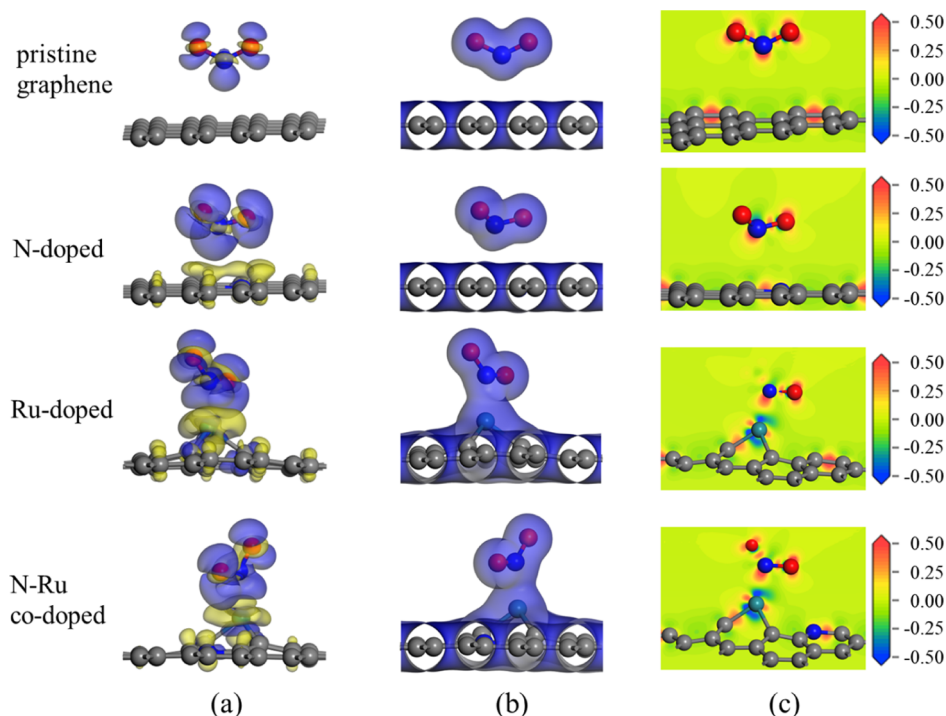


Figure 3. (a) Charge density difference, (b) total charge density, and (c) electron density difference plots of NO_2 molecules adsorbed on the different graphene surfaces. The isosurfaces of the charge density difference plots are set to $0.01 \text{ e}/\text{\AA}^3$, where blue represents electron accumulation and yellow represents electron depletion. The isosurfaces of the total charge density plots are set to $0.02 \text{ e}/\text{\AA}^3$. In the electron density difference plots, red represents charge accumulation and blue represents charge depletion.

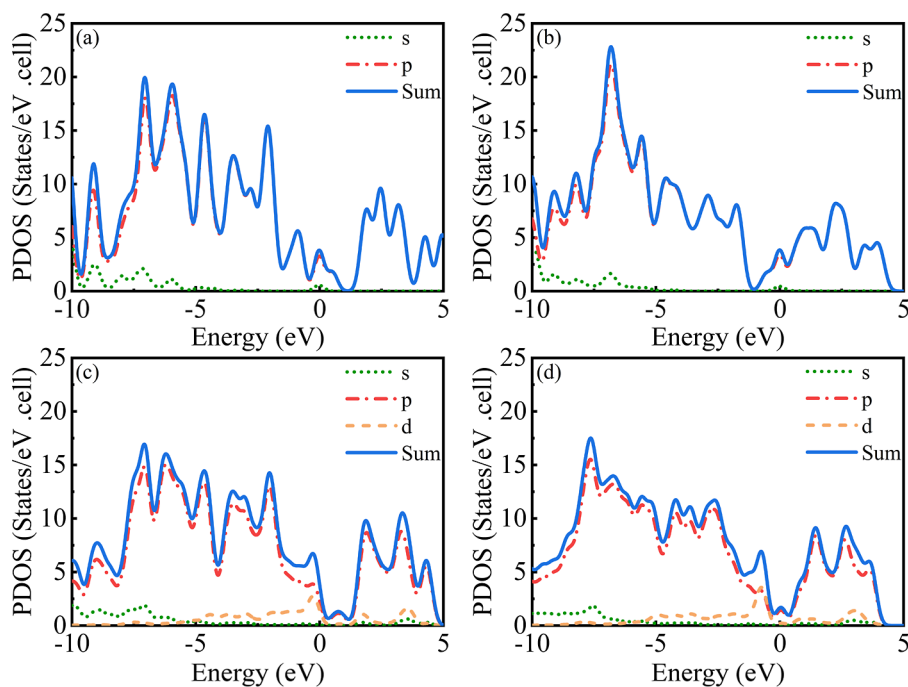


Figure 4. Partial density of states (PDOS) of adsorbed NO_2 molecules on the graphene surfaces. (a) Pristine graphene, (b) N-doped graphene, (c) Ru-doped graphene, and (d) N–Ru-co-doped graphene.

described by the dielectric function. This is because the electron jump energy is much larger than the energy of phonon perturbation, so the effect of the perturbation of the radiated electric field on the electron absorption of the photon energy from low to high energy levels can be ignored. The real and imaginary parts of the dielectric function describe the

processes of photon absorption and release in a material. The complex form $\epsilon(\omega) = \epsilon_1(\omega) + i\epsilon_2(\omega)$ describes the process of electron migration, where ω is the angular frequency, $\epsilon_1 = n^2 - k^2$ and $\epsilon_2 = 2nk$, in which n is the refractive index and k is the wavenumber.³⁷ The real and imaginary parts of the dielectric function can be derived from

the Kramers–Kronig dispersion relation. In addition, the absorption coefficient $I(\omega)$ and reflectivity $R(\omega)$ can be derived from the Kramers–Kronig dispersion relation as follows³⁸

$$I(\omega) = \sqrt{2} \omega [\sqrt{\varepsilon_1^2(\omega) - \varepsilon_2^2(\omega)} - \varepsilon_1(\omega)]^{1/2} \quad (3)$$

$$R(\omega) = \left| \frac{\sqrt{\varepsilon_1(\omega) + i\varepsilon_2(\omega)} - 1}{\sqrt{\varepsilon_1(\omega) + i\varepsilon_2(\omega)} + 1} \right|^2 \quad (4)$$

The imaginary parts of the dielectric functions before and after NO₂ adsorption on the different graphene surfaces in the visible range (1.6–3.2 eV) are shown in Figure 5. Within the

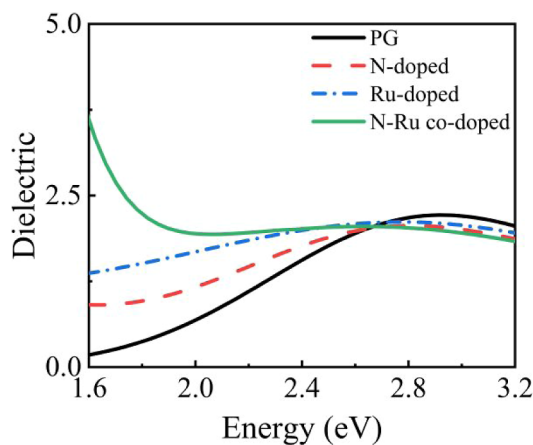


Figure 5. Imaginary parts of the dielectric functions of the different graphene surfaces after adsorption of NO₂.

energy range of 1.6–2.6 eV, the imaginary part values on the doped graphene surfaces are higher than those on the pristine graphene surface, with Ru–N-*co*-doped graphene exhibiting the highest value. In the energy range of 2.6–3.2 eV, the imaginary part values of the doped graphene surfaces are slightly smaller than those of the pristine graphene surface, with Ru–N-*co*-doped graphene showing the smallest imaginary part value. Therefore, in the visible range, the Ru–N-*co*-doped graphene surface exhibits the largest variation of the imaginary part of the dielectric function among the graphene-based surfaces.

The absorption rate is directly related to the number of electrons in the ground state that absorb photon energy and transition to the excited state. This phenomenon reflects the ability of a material to respond to light. Similarly, higher $R(\omega)$ indicates that more electrons absorb photon energy and transition to an excited state, which is followed by the release of energy as they transition back to lower energy levels.

The calculated absorption and reflection spectra of NO₂ molecules adsorbed on the different graphene surfaces are shown in Figure 6a,b, respectively. In the visible range, the peak absorption coefficient of the pristine graphene surface of approximately 39,200 cm⁻¹ occurs at 3.2 eV and the peak reflection coefficient of approximately 0.12 occurs at 3 eV. The optical properties of the N-doped and Ru-doped graphene surfaces with adsorbed NO₂ are similar to those of pristine graphene with adsorbed NO₂. However, N–Ru codoping greatly affects the optical properties of the graphene surface with adsorbed NO₂. The N–Ru-*co*-doped system exhibits a peak absorption coefficient of approximately 112,900 cm⁻¹ at

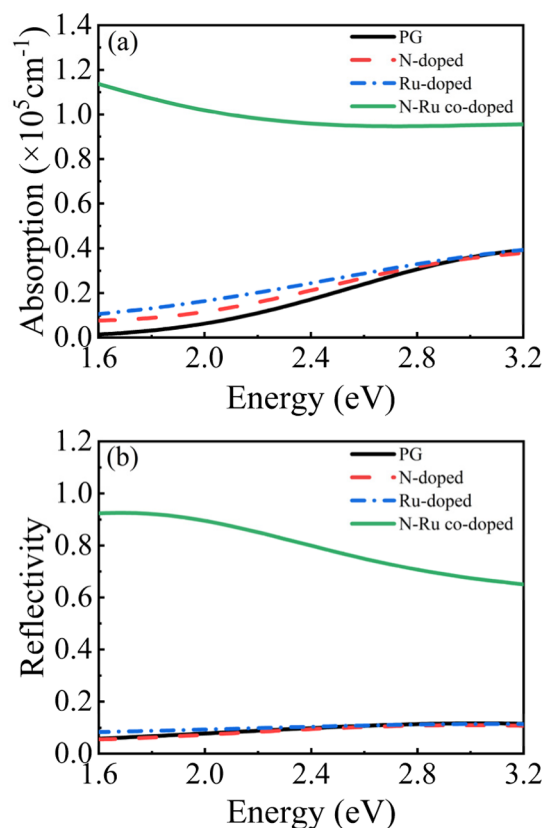


Figure 6. Optical properties of the different graphene surfaces after adsorption of NO₂. (a) Absorption spectra and (b) reflection spectra.

1.6 eV and a peak reflection coefficient of approximately 0.93 at 1.7 eV. These values are approximately 2.88 and 7.75 times higher than the corresponding peak absorption and reflection coefficients of pristine graphene, respectively. Therefore, the N–Ru-*co*-doped graphene system shows superior optical sensing capability for NO₂ to pristine graphene. The trend is the same for the optical properties of the other two adsorption sites (B and T sites) (see Figures S9 and S10).

A comparative analysis of the dielectric functions, absorption spectra, and reflection spectra of NO₂ molecules adsorbed on the different graphene surfaces revealed that the trends in the absorption and reflection spectra are consistent with the changes of the dielectric function. In particular, N–Ru codoping markedly enhances the optical properties of NO₂ adsorbed on the graphene surface, particularly within the visible range.

4. CONCLUSION

In this study, we performed DFT-based first-principles calculations to investigate the adsorption behavior of NO₂ gas molecules on pristine, metal-doped, nonmetal-doped, and metal–nonmetal-*co*-doped graphene surfaces. Various properties, including the adsorption energy, Mulliken charge distribution, differential charge density, DOS, and optical properties, were examined to characterize the interaction between NO₂ and the different graphene surfaces. The results indicated that NO₂ can adsorb to all four types of graphene, with the doped graphene surfaces showing stronger NO₂ adsorption than pristine graphene. Pristine and N-doped graphene show physical adsorption of NO₂, whereas the introduction of transition metal atoms, such as Ru, leads to

strong chemical adsorption because of the formation of chemical bonds between NO₂ and the doped graphene surfaces. The N–Ru-co-doped system shows the highest adsorption energy of –7.41 eV. Comparison of the DOS revealed that doped graphene materials are more sensitive to NO₂ gas molecules than pristine graphene. The electronic properties of graphene change upon NO₂ adsorption, and the optical properties of the doped graphene surfaces are improved compared with those of pristine graphene. Notably, the N–Ru-co-doped graphene surface exhibits the largest changes in the absorption and reflectance coefficients upon NO₂ adsorption, which are approximately 2.88 and 7.75 times higher than those of pristine graphene, respectively. The substantial changes in the electronic and optical properties of N–Ru-co-doped graphene upon interaction with NO₂ make it a promising candidate for NO₂ gas detection applications.

■ ASSOCIATED CONTENT

SI Supporting Information

The Supporting Information is available free of charge at <https://pubs.acs.org/doi/10.1021/acsomega.4c09163>.

Data on adsorption energy, density of states, differential charge density, and optical properties of NO₂ molecules adsorbed on graphene surfaces (T-site and B-site), among others (PDF)

■ AUTHOR INFORMATION

Corresponding Authors

Hongqiang Zhu – College of Physics and Electronic Engineering, Chongqing Normal University, Chongqing 401331, China; orcid.org/0000-0002-2056-7923; Email: 20132013@cqnu.edu.cn

Weiyao Jia – School of Physical Science and Technology, Southwest University, Chongqing 400715, China; Email: wyjia@swu.edu.cn

Authors

Lei Luo – College of Physics and Electronic Engineering, Chongqing Normal University, Chongqing 401331, China
Kaihui Yin – College of Physics and Electronic Engineering, Chongqing Normal University, Chongqing 401331, China
Zebang Wu – College of Physics and Electronic Engineering, Chongqing Normal University, Chongqing 401331, China
Fengxia Xu – College of Physics and Electronic Engineering, Chongqing Normal University, Chongqing 401331, China
Tianjun Gao – College of Physics and Electronic Engineering, Chongqing Normal University, Chongqing 401331, China
Yuanxia Yue – College of Physics and Electronic Engineering, Chongqing Normal University, Chongqing 401331, China
Jianjun Chen – School of Microelectronics and Communication Engineering, Chongqing University, Chongqing 400044, China
Qing Feng – College of Physics and Electronic Engineering, Chongqing Normal University, Chongqing 401331, China
Ying Yang – College of Physics and Electronic Engineering, Chongqing Normal University, Chongqing 401331, China

Complete contact information is available at: <https://pubs.acs.org/doi/10.1021/acsomega.4c09163>

Notes

The authors declare no competing financial interest.

■ ACKNOWLEDGMENTS

This work was supported by the Natural Science Foundation of Chongqing, China (grant nos. CSTB2023NSCQ-MSX0207 and CSTB2023NSCQ-MSX0425), the Science and Technology Research Program of Chongqing Municipal Education Commission, China (grant nos. KJQN202200569, KJQN202200507 and KJQN202300513), the Scientific and Technological Research Program of Chongqing Municipal Education Commission, China (grant no. KJZD-K202300516), the Higher Education Teaching Reform Research Project of Chongqing, China (grant no. 223145), and the “Curriculum Ideological and Political” Demonstration Project of Chongqing Municipal Education Commission, China (grant no. YKCSZ23102). We thank Liwen Bianji (Edanz) (www.liwenbianji.cn/) for editing the English text of a draft of this manuscript.

■ REFERENCES

- (1) Cooper, M. J.; Martin, R. V.; Hammer, M. S.; Levelt, P. F.; Veefkind, P.; Lamsal, L. N.; Krotkov, N. A.; Brook, J. R.; McLinden, C. A. Global fine-scale changes in ambient NO₂ during COVID-19 lockdowns. *Nature* **2022**, *601*, 380–387.
- (2) Lim, H.; Kwon, H.; Kang, H.; Jang, J. E.; Kwon, H. J. Semiconducting MOFs on ultraviolet laser-induced graphene with a hierarchical pore architecture for NO₂ monitoring. *Nat. Commun.* **2023**, *14*, 3114.
- (3) Abbasi, A.; Sardroodi, J. J. A highly sensitive chemical gas detecting device based on N-doped ZnO as a modified nanostructure media: A DFT plus NBO analysis. *Surf. Sci.* **2018**, *668*, 150–163.
- (4) Kang, S. G.; Choi, W. M. Predicting the adsorption and reduction of NO₂ on Sr-doped CeO₂(111) using first-principles calculations. *Appl. Surf. Sci.* **2023**, *612*, 155896.
- (5) Kuang, A. L.; Mo, M.; Kuang, M. Q.; Wang, B.; Tian, C. L.; Yuan, H. K.; Wang, G. Z.; Chen, H. The comparative study of XO₂ (X = C, N, S) gases adsorption and dissociation on pristine and defective graphene supported Pt₁₃. *Mater. Chem. Phys.* **2020**, *247*, 122712.
- (6) Almaraz, M.; Bai, E.; Wang, C.; Trousdell, J.; Conley, S.; Faloua, I.; Houlton, B. Z. Agriculture is a major source of NO_x pollution in California. *Sci. Adv.* **2018**, *4*, 3477.
- (7) Geng, X.; Li, S. W.; Mawella-Vithanage, L.; Ma, T.; Kilani, M.; Wang, B. W.; Ma, L.; Hewa-Rahinduwage, C. C.; Shafikova, A.; Nikolla, E.; Mao, G. Z.; Brock, S. L.; Zhang, L.; Luo, L. Atomically dispersed Pb ionic sites in PbCdSe quantum dot gels enhance room-temperature NO₂ sensing. *Nat. Commun.* **2021**, *12*, 4895.
- (8) Kang, S. G. First-principles prediction of NO₂ and SO₂ adsorption on MgO/(Mg_{0.5}Ni_{0.5})O/MgO(100). *Appl. Surf. Sci.* **2021**, *566*, 150650.
- (9) Abbasi, A.; Sardroodi, J. J. Adsorption of O₃, SO₂ and SO₃ gas molecules on MoS₂ monolayers: A computational investigation. *Appl. Surf. Sci.* **2019**, *469*, 781–791.
- (10) Abbasi, A. Tuning the structural and electronic properties and chemical activities of stanene monolayers by embedding 4d Pd: a DFT study. *RSC Adv.* **2019**, *9*, 16069–16082.
- (11) Abbasi, A.; Sardroodi, J. J. Exploration of sensing of nitrogen dioxide and ozone molecules using novel TiO₂/Stanene heterostructures employing DFT calculations. *Appl. Surf. Sci.* **2018**, *442*, 368–381.
- (12) Zhang, F. Z.; Yang, K.; Liu, G. J.; Chen, Y.; Wang, M. H.; Li, S. T.; Li, R. F. Recent advances on graphene: Synthesis, properties and applications. *Composites, Part A* **2022**, *160*, 107051.
- (13) Abbasi, A.; Sardroodi, J. J. An Innovative Method for the Removal of Toxic SO_x Molecules from Environment by TiO₂/Stanene Nanocomposites: A First-Principles Study. *J. Inorg. Organomet. Polym.* **2018**, *28*, 1901–1913.
- (14) Abbasi, A.; Abdelrasoul, A.; Sardroodi, J. J. Adsorption of CO and NO molecules on Al, P and Si embedded MoS₂ nanosheets investigated by DFT calculations. *Adsorption* **2019**, *25*, 1001–1017.

- (15) Kuang, A. L.; Kuang, M. Q.; Yuan, H. K.; Wang, G. Z.; Chen, H.; Yang, X. L. Acidic gases (CO₂, NO₂ and SO₂) capture and dissociation on metal decorated phosphorene. *Appl. Surf. Sci.* **2017**, *410*, 505–512.
- (16) Jang, A. R.; Lim, J. E.; Jang, S.; Kang, M. H.; Lee, G.; Chang, H.; Kim, E.; Park, J. K.; Lee, J. O. Ag₂S nanoparticles decorated graphene as a selective chemical sensor for acetone working at room temperature. *Appl. Surf. Sci.* **2021**, *562*, 150201.
- (17) Esfahani, S.; Akbari, J.; Soleimani-Amiri, S.; Mirzaei, M.; Ghasemi Gol, A. Assessing the drug delivery of ibuprofen by the assistance of metal-doped graphenes: Insights from density functional theory. *Diam. Relat. Mater.* **2023**, *135*, 109893.
- (18) Cruz-Martínez, H.; Rojas-Chávez, H.; Montejo-Alvaro, F.; Peña-Castañeda, Y. A.; Matadamas-Ortiz, P. T.; Medina, D. I. Recent Developments in Graphene-Based Toxic Gas Sensors: A Theoretical Overview. *Sensors* **2021**, *21*, 1992.
- (19) Shamim, S. U. D.; Roy, D.; Alam, S.; Piya, A. A.; Rahman, M. S.; Hossain, M. K.; Ahmed, F. Doubly doped graphene as gas sensing materials for oxygen-containing gas molecules: A first-principles investigation. *Appl. Surf. Sci.* **2022**, *596*, 153603.
- (20) Yang, B.; Li, D. B.; Qi, L.; Li, T. B.; Yang, P. Thermal properties of triangle nitrogen-doped graphene nanoribbons. *Phys. Lett. A* **2019**, *383*, 1306–1311.
- (21) Zhu, P. C.; Tang, F.; Wang, S. F.; Cao, W.; Wang, Q. Adsorption performance of CNCl, NH₃ and GB on modified graphene and the selectivity in O₂ and N₂ environment. *Mater. Today Commun.* **2022**, *33*, 104280.
- (22) Jia, X. T.; Zhang, H.; Zhang, Z. M.; An, L. B. First-principles investigation of vacancy-defected graphene and Mn-doped graphene towards adsorption of H₂S. *Superlattices Microstruct.* **2019**, *134*, 106235.
- (23) Jia, X.; An, L. The adsorption of nitrogen oxides on noble metal-doped graphene: The first-principles study. *Mod. Phys. Lett. B* **2019**, *33*, 1950044.
- (24) Choudhuri, I.; Patra, N.; Mahata, A.; Ahuja, R.; Pathak, B. B-N@Graphene: Highly Sensitive and Selective Gas Sensor. *J. Phys. Chem. C* **2015**, *119*, 24827–24836.
- (25) Zou, Y.; Li, F.; Zhu, Z. H.; Zhao, M. W.; Xu, X. G.; Su, X. Y. An ab initio study on gas sensing properties of graphene and Si-doped graphene. *Eur. Phys. J. B* **2011**, *81*, 475–479.
- (26) Odey, D. O.; Edet, H. O.; Louis, H.; Gber, T. E.; Nwagu, A. D.; Adaliku, S. A.; Adeyinka, A. S. Heteroatoms (B, N, and P) doped on nickel-doped graphene for phosgene (COCl₂) adsorption: insight from theoretical calculations. *Mater. Today Sustain.* **2023**, *21*, 100294.
- (27) Dai, J.; Yuan, J.; Giannozzi, P. Gas adsorption on graphene doped with B, N, Al, and S: A theoretical study. *Appl. Phys. Lett.* **2009**, *95*, 232105.
- (28) Zhang, T.; Sun, H.; Wang, F. G.; Zhang, W. Q.; Tang, S. W.; Ma, J. M.; Gong, H. W.; Zhang, J. P. Adsorption of phosgene molecule on the transition metal-doped graphene: First principles calculations. *Appl. Surf. Sci.* **2017**, *425*, 340–350.
- (29) Nasehnia, F.; Seifi, M. Adsorption of molecular oxygen on VIIIIB transition metal doped graphene: A DFT study. *Mod. Phys. Lett. B* **2014**, *28*, 1450237.
- (30) Liang, X. Y.; Ding, N.; Ng, S. P.; Wu, C. M. L. Adsorption of gas molecules on Ga-doped graphene and effect of applied electric field: A DFT study. *Appl. Surf. Sci.* **2017**, *411*, 11–17.
- (31) Zhang, H. P.; Luo, X. G.; Lin, X. Y.; Lu, X.; Leng, Y.; Song, H. T. Density functional theory calculations on the adsorption of formaldehyde and other harmful gases on pure, Ti-doped, or N-doped graphene sheets. *Appl. Surf. Sci.* **2013**, *283*, 559–565.
- (32) Basiuk, V. A.; Henao-Holguin, L. V. Dispersion-corrected density functional theory calculations of meso-tetraphenylporphine-C₆₀ complex by using DMol3 module. *J. Comput. Theor. Nanosci.* **2014**, *11*, 1609–1615.
- (33) Yang, Z. H.; Wang, Z. Y.; Su, X. P. First-principles investigation of cohesive energy and electronic structure in vanadium phosphides. *J. Cent. South Univ.* **2012**, *19*, 1796–1801.
- (34) Ma, L.; Zhang, J. M.; Xu, K. W.; Ji, V. A first-principles study on gas sensing properties of graphene and Pd-doped graphene. *Appl. Surf. Sci.* **2015**, *343*, 121–127.
- (35) Duan, J. Y.; Liu, Y.; Chen, Y. M. Enhancement of SO₂ sensing performance of micro-ribbon graphene sensors using nitrogen doping and light exposure. *Appl. Surf. Sci.* **2023**, *608*, 155059.
- (36) Gao, X.; Zhou, Q.; Wang, J. X.; Xu, L. N.; Zeng, W. Adsorption of SO₂ molecule on Ni-doped and Pd-doped graphene based on first-principle study. *Appl. Surf. Sci.* **2020**, *517*, 146180.
- (37) Tong, Z.; Dumitrica, T.; Frauenheim, T. First-principles prediction of infrared phonon and dielectric function in biaxial hyperbolic van der Waals crystal α -MoO₃. *Phys. Chem. Chem. Phys.* **2021**, *23*, 19627–19635.
- (38) Ping, L. K.; Mohamed, M. A.; Mondal, A. K.; Taib, M. F. M.; Samat, M. H.; Berhanuddin, D. D.; Menon, P. S.; Bahru, R. First-Principles Studies for Electronic Structure and Optical Properties of Strontium Doped β -Ga₂O₃. *Micromachines* **2021**, *12* (4), 348.